

Evidence for forward scattering and coupling to acoustic phonon modes in high- T_c cuprate superconductors

S. Johnston^{1,4}, I. M. Vishik^{1,2,3}, W. S. Lee^{1,2}, F. Schmitt^{1,2}, S. Uchida⁵, K. Fujita⁶, S. Ishida⁵, N. Nagaosa^{7,8}, Z. X. Shen^{1,2,3}, and T. P. Devereaux^{1,2}

¹*Stanford Institute for Materials and Energy Science,*

SLAC National Accelerator Laboratory and Stanford University, Stanford, CA 94305, USA

²*Geballe Laboratory for Advanced Materials, Stanford University, Stanford, CA 94305, USA*

³*Department of Physics and Applied Physics, Stanford University, Stanford, CA 94305, USA*

⁴*IFW Dresden, P.O. Box 27 01 16, D-01171 Dresden, Germany*

⁵*Department of Physics, Graduate School of Science,*

University of Tokyo, Bunkyo-Ku, Tokyo 113-0033, Japan

⁶*Laboratory for Atomic and Solid State Physics, Department of Physics,
Cornell University, Ithaca, New York 14853, USA*

⁷*Department of Applied Physics, University of Tokyo, Bunkyo-ku, Tokyo 113-8656, Japan and*

⁸*Cross-Correlated Materials Research Group (CMRG) and Correlated
Electron Research Group (CERG), RIKEN-ASI, Wako 351-0198, Japan*

(Dated: October 28, 2018)

Recent laser angle-resolved photoemission spectroscopy studies have established the presence of a new kink in the low-energy nodal dispersion of $\text{Bi}_2\text{Sr}_2\text{CaCu}_2\text{O}_{8+\delta}$ (Bi-2212). The energy scale ($\sim 8 - 15$ meV) of this kink appears below the maximum of the superconducting gap Δ_0 . Therefore it is difficult to interpret this feature in terms of the usual coupling to a sharp dispersionless mode. In this paper we examine electron-phonon coupling to the in-plane acoustic phonon branch arising from the modulation of the screened Coulomb potential. We demonstrate that such a coupling has a strong forward scattering peak, and as a consequence, a kink occurs in the dispersion at an energy scale shifted by the local gap $\Delta(\mathbf{k})$. In addition, considerations for the reduction of screening with underdoping naturally explains the observed doping dependence of the low-energy kink. These results point to a strong coupling to the acoustic branch which is peaked in the forward scattering direction and has important implications for transport and pairing in the high- T_c cuprates.

PACS numbers: 71.38.-k, 74.72.-h, 74.25.Jb

Understanding what controls the superconducting transition temperature T_c in the cuprates remains one of the major questions in condensed matter physics. The large variation in T_c across cuprate families remains unexplained despite the near similarity of the CuO_2 plane and accompanying strong correlation physics that well describes the parent phases of these systems. Strong electron correlations are of course important in all the transition metal oxides, but the cuprates are special in the sense that they are the most metallic system among them. As a result, the cuprates are at the verge of localization/delocalization and/or ionicity/covalency. This subtle balance or dichotomy may be key to the origin of the robust superconductivity, which requires both strong coupling and quantum coherence.

This battleground has recently been highlighted in angle-resolved photoemission (ARPES), where polaronic lattice effects demonstrably alter the spectral function from a Lorentzian to Gaussian lineshape^{1,2} in undoped systems. The presence of dispersion "kinks" in doped cuprates have been (controversially) interpreted as coupling to lattice phonons, with stronger couplings than implied by density functional calculations.³⁻⁵ Finally, with the advancements of laser-based ARPES, a new energy scale has been observed in the nodal region of $\text{Bi}_2\text{Sr}_2\text{CaCu}_2\text{O}_{8+\delta}$ (Bi-2212) which manifests as a subtle kink in the band dispersion at an energy 8-15 meV.⁶⁻¹⁰

In this paper, we focus on the latter kink in underdoped Bi-2212 ($T_c = 55\text{K}$, UD55, $p \sim 0.088$) and present

data and analysis which suggests that the interplay of Coulomb interactions and lattice effects as a consequence of ionicity/covalency dichotomy plays an important role in the physics of a doped Mott insulator. The experimental setup is identical to Ref. 9. The energy resolution was 3 meV and no deconvolution methods have been applied to the data.⁷ Whereas previous studies focused on the low-energy kink at the node, we have done experiments away from the node where the gap is nonzero. Since the opening of a gap will affect the momentum distribution curve (MDC) dispersion close to the gap energy, we chose a doping where the low-energy kink is very strong (Ref. 9) so the two features can be easily distinguished. However, we emphasize that the results presented here hold for other dopings in the underdoped regime.

The main experimental observations for the low-energy kink along the nodal direction are summarized in Fig. 1. As evident in the raw data (Fig. 1a), the kink manifests as a bend in the dispersion and an accompanying change in spectral intensity at an energy $\sim 8-15$ meV in UD55 Bi-2212. This behavior is also evident in the MDC derived dispersion, which deviates from the linear dispersion at the same energy scale (Figs. 1b). For UD55, the slope of the dispersion at E_f is considerably smaller than the slope of the dispersion between 30-40 meV (v_{mid}) and the low-energy kink is unmistakable. This observation has already been discussed in the context of the universal nodal Fermi velocity,⁹ suggesting the importance of this new energy scale in the low-energy nodal physics

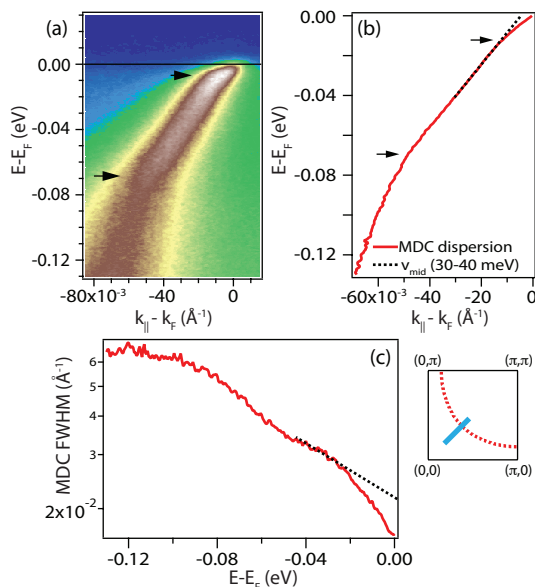


FIG. 1: (Color online) Nodal low-energy kink in Bi-2212 UD55. (a) Color image plot of raw data. The 70 meV and low-energy kinks are marked by arrows and both can be seen by eye in the raw data via a bend in the dispersion and an accompanying change in spectral intensity. (b) Band dispersion derived by fitting the momentum distribution curve (MDCs, intensity as a function of momentum at fixed energy) at each energy in (a) to a Lorentzian. The low-energy kink is defined by the deviation of the dispersion from v_{mid} , the velocity fit between 30-40 meV (dotted line). (c) MDC FWHM shows a more rapid decrease close to E_f as a consequence of the low-energy kink.

of the high- T_c cuprates. A corresponding signature is also seen in the MDC FWHM, which shows a more rapid decrease for energies below the low-energy kink. Additionally, these features have been observed over a wide doping range in underdoped Bi-2212, strengthening with underdoping, suggesting that it may be a ubiquitous aspect of nodal physics.⁹

The 70 meV kink has been interpreted in terms of coupling to a sharp bosonic mode of energy Ω which is of either a lattice¹⁰⁻¹⁴ or magnetic¹⁵⁻¹⁸ origin. By analogy, it has been suggested that the low-energy kink can be interpreted as coupling to an optical phonon.⁷ In Bi-2212 there are known infrared active optical modes at 97 (12) and 117 cm^{-1} (14.5 meV) involving c -axis motion of the Cu, Ca, Sr and Bi ions¹⁹ as well as a Raman active c -axis optical branch between 58 and 65 cm^{-1} (7.2 and 8.1 meV) with the latter recently invoked to explain the low-energy kink.⁷ However, coupling to these optical modes is likely to be electrostatic in nature and therefore not sharply peaked in momentum space. Such a coupling would produce a kink at $\Omega + \Delta_0$.^{13-15,20} However, it is possible to have a non-gap-shifted feature in the self-energy near the node if the coupling is strongly peaked in the forward scattering direction.²¹ Such is the case for the in-plane acoustic mode, which we consider here.

The generic form for the el-ph coupling Hamiltonian is

given by

$$H_{el-ph} = \frac{1}{\sqrt{N}} \sum_{\mathbf{k}, \mathbf{q}, \sigma, \nu} |g_{\mu}(\mathbf{k}, \mathbf{q})|^2 d_{\mathbf{k}-\mathbf{q}, \sigma}^{\dagger} d_{\mathbf{k}, \sigma} (b_{\mathbf{q}, \nu}^{\dagger} + b_{-\mathbf{q}, \nu}) \quad (1)$$

where $d_{\mathbf{k}, \sigma}^{\dagger}$ ($d_{\mathbf{k}, \sigma}$) creates (annihilates) an electron in the antibonding $pd - \sigma^*$ band with momentum \mathbf{k} and spin σ and $b_{\mathbf{q}, \nu}^{\dagger}$ ($b_{\mathbf{q}, \nu}$) creates (annihilates) a phonon quanta of momentum \mathbf{q} in branch ν . For the in-plane acoustic coupling, the el-ph interaction arises via a deformation-type coupling of the periodic lattice potential. In this case, momentum-dependent el-ph coupling constant $g(\mathbf{k}, \mathbf{q})$ is only a function of \mathbf{q} and is given by²²

$$g(\mathbf{q}) = \frac{1}{V_{cell}} \sqrt{\frac{\hbar}{2M\Omega(\mathbf{q})}} \hat{\epsilon}_{\mathbf{q}} \cdot \mathbf{q} \frac{V(\mathbf{q})}{\epsilon(\mathbf{q})} \quad (2)$$

with $\Omega(\mathbf{q})$ the phonon dispersion, $\epsilon(\mathbf{q}) = 1 + q_{TF}^2/q^2$ the Thomas-Fermi dielectric function, q_{TF} the Thomas-Fermi wavevector, $V_{cell} = a^2c$ the unit cell volume, M the copper + oxygen ion mass, $\hat{\epsilon}_{\mathbf{q}}$ the phonon polarization vector and $V(\mathbf{q}) = 4\pi e^2/q^2\epsilon$ the Coulomb potential with ϵ the static dielectric constant.

Apart from the dispersion of $\Omega(\mathbf{q})$, Eq. (2) has a \mathbf{q} -dependence governed by $\propto \hat{\epsilon}_{\mathbf{q}} \cdot \mathbf{q}/(q^2 + q_{TF}^2)$ which is strongly peaked for $q \sim q_{TF}$ but with $g(\mathbf{q}) \rightarrow 0$ for $\mathbf{q} \rightarrow 0$. In the underdoped cuprates the Thomas-Fermi wavevector is small and $|g(\mathbf{q})|^2$ is sharply peaked for a subset of small \mathbf{q} .²³ As a result, the el-ph self-energy is dominated by contributions from scattering process from states $E_{\mathbf{k}}$ to nearby states $E_{\mathbf{k}+\mathbf{q}}$, with $E^2(\mathbf{k}) = \xi^2(\mathbf{k}) + \Delta^2(\mathbf{k})$, where $\xi(\mathbf{k}) = \epsilon(\mathbf{k}) - \mu$ is the electron dispersion in the normal state measured relative to the Fermi level.²⁴ The nodal self-energy is thus determined from scattering to nearby states with a small superconducting gap and thus the peak in the self-energy is not shifted by the full gap but rather an average of the gap near the node.

To demonstrate this we now calculate the spectral function for coupling to the acoustic phonon branch with $\Omega(\mathbf{q}) = \Omega_0 \sqrt{\sin^2(q_x a/2) + \sin^2(q_y a/2)}/\sqrt{2}$ and $\Omega_0 = 15$ meV.²⁵ We also include coupling to the 55 and 36 meV in- and out-of-phase c -axis polarized modes (the so-called A_{1g} and B_{1g} branches, respectively), as well as the 70 meV Cu-O bond-stretching modes in order to also capture the well-known 70 meV kink and renormalizations at higher binding energy. Since our focus is on the features at low energy, we treat the optical modes as dispersionless with a momentum-independent coupling. The superconducting gap is modelled with a pure d -wave form $\Delta(\mathbf{k}) = \Delta_0[\cos(k_x a) - \cos(k_y a)]/2$, where $\Delta_0 = 37$ meV is the maximum value at $(0, \pi)$. We take the dielectric constant to be set by a large in-plane value with $\epsilon = 30\epsilon_0$ (in this context we regard ϵ as a free parameter set to obtain overall agreement with experiment) and take $q_{TF} = 0.5\pi/a$. Finally, we take the effective lattice constants per plane to be $a = b = 3.8$ and $c = 7.65$ Å, appropriate for Bi-2212.¹⁹ The self-energy $\Sigma(\mathbf{k}, \omega)$ and spectral function $A(\mathbf{k}, \omega)$ are calculated within Migdal-Eliashberg theory, which is the same formalism used in prior work to

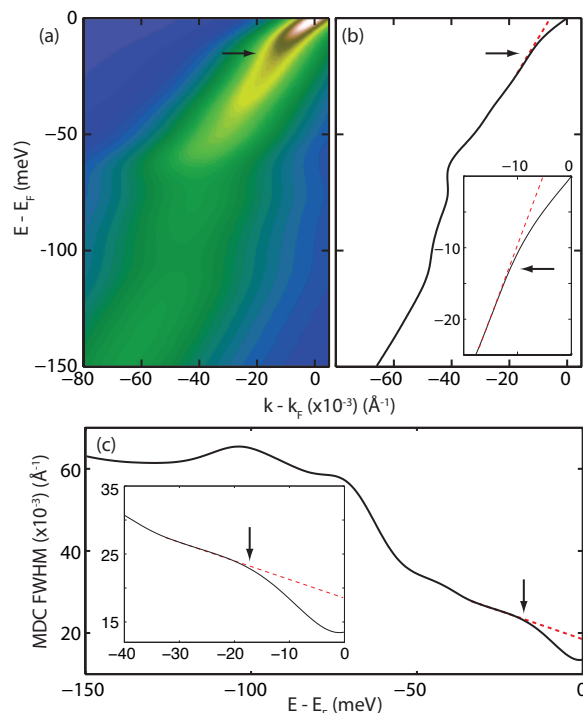


FIG. 2: (Color online) (a) The calculated spectral function $A(\mathbf{k}, \omega)$ along the nodal direction $(0,0)-(\pi,\pi)$ of superconducting (25 K) Bi-2212. (b) The MDC-derived dispersion and (c) MDC FWHM obtained from the calculated $A(\mathbf{k}, \omega)$. In calculating $A(\mathbf{k}, \omega)$, an additional component $\propto \omega^2$ has been added to the imaginary part of the self-energy in order to simulate additional broadening due to el-el interactions.

understand the higher energy renormalizations^{13,14,23}. In order to introduce increased broadening in the spectral function with underdoping, we evaluate the self-energies while adding a finite imaginary part ($\delta = 7$ meV) to the bare electron Green's function.

The strength of the el-ph coupling can be estimated from the slope of the self-energy at the Fermi level

$$\lambda(\mathbf{k}) = - \left. \frac{\partial \text{Re}\Sigma(\mathbf{k}, \omega)}{\partial \omega} \right|_{\omega=0}. \quad (3)$$

For the above choice of parameters we obtain $\lambda(\mathbf{k}_{node}) = 0.56$ for the acoustic branch, consistent with the observed magnitude of the renormalization.^{9,10} For the optical modes we set the overall strength such that $\lambda_z = 0.23, 0.05$ and 0.05 for the 36, 55 and 70 meV modes, respectively, in order to match previous work.^{13,23}

The calculated $A(\mathbf{k}, \omega)$ (and corresponding MDC analysis) for nodal cut in the superconducting state (25 K) is shown in Fig. 2. As with the experimental data (Fig. 1), the low energy kink is evident in the raw spectral function appearing at an energy set by the phonon dispersion weighted by $g(\mathbf{q})$. Since the coupling for scattering to the antinode is suppressed, this energy scale is slightly smaller than the van Hove points in the phonon density of states (10.6 and 15 meV). The low-energy kink is also evident in the MDC-derived dispersion and linewidth, shown in Figs. 2b and 2c, respectively. Both are in ex-

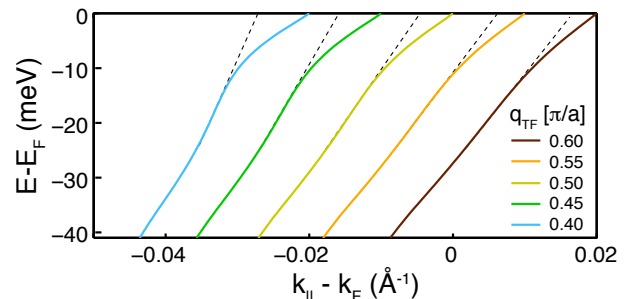


FIG. 3: Nodal MDC derived dispersions obtained from the model $A(\mathbf{k}, \omega)$ for various values of the Thomas-Fermi wavevector. The value of the dielectric constant ϵ has been held fixed for each case.

cellent agreement with the experimental data (Fig. 1), demonstrating that the forward scattering nature of the coupling to the acoustic branch accounts for both the energy scale of the low-energy kink and the overall strength of the renormalization near the Fermi level.

Since the coupling to the acoustic mode arises from the modulation of the screened Coulomb interaction a doping dependence naturally emerges from the increased metallicity of the cuprates with overdoping.²³ To examine the implications of this, in Fig. 3 we plot nodal MDC-derived dispersions obtained for our model calculations while varying q_{TF} from $0.4\pi/a$ to $0.6\pi/a$. This allows us to mimic the increased screening which occurs with progressive overdoping. For decreasing q_{TF} the overall strength of the coupling increases and becomes increasingly peaked at small \mathbf{q} . As a result, stronger kinks are produced with underdoping in agreement with experiment.⁹ We also note that increased coupling at small \mathbf{q} with underdoping has also been reported for more a complicated form for the dielectric function based on RPA treatments²³ and is therefore expected to be a generic result. These effects are also expected to survive the inclusion of the short-range Hubbard interaction, which largely suppresses the el-ph vertex at large \mathbf{q} over its value at small \mathbf{q} .²⁶

We now turn our attention to the momentum dependence of the low-energy kink. As previously mentioned, for small q_{TF} the el-ph self-energy is dominated by scattering to nearby momentum states and thus samples the local \mathbf{k} -space value of the superconducting gap. Therefore, for off-nodal cuts, the energy of the kink should begin to gap shift, following the local value of $\Delta(\mathbf{k})$ for each cut. In Figs. 4a and 4b we present experimental and calculated MDC-derived dispersions for a series of off-nodal cuts in a direction parallel to $(0,0)-(\pi,\pi)$ with cuts taken up to 11 degrees away from the node. Experimentally, the superconducting gap is determined independently for each cut by fitting symmetrized energy distribution curves at k_F to a minimal model proposed by Norman *et al.*²⁷ In Fig. 4a the kink position is determined from the deviation of the a straight line determined from fitting the dispersion slope v_{mid} between 30-40 meV. The parameters for the calculations (Fig. 4b) are identical to those used in Fig. 2.

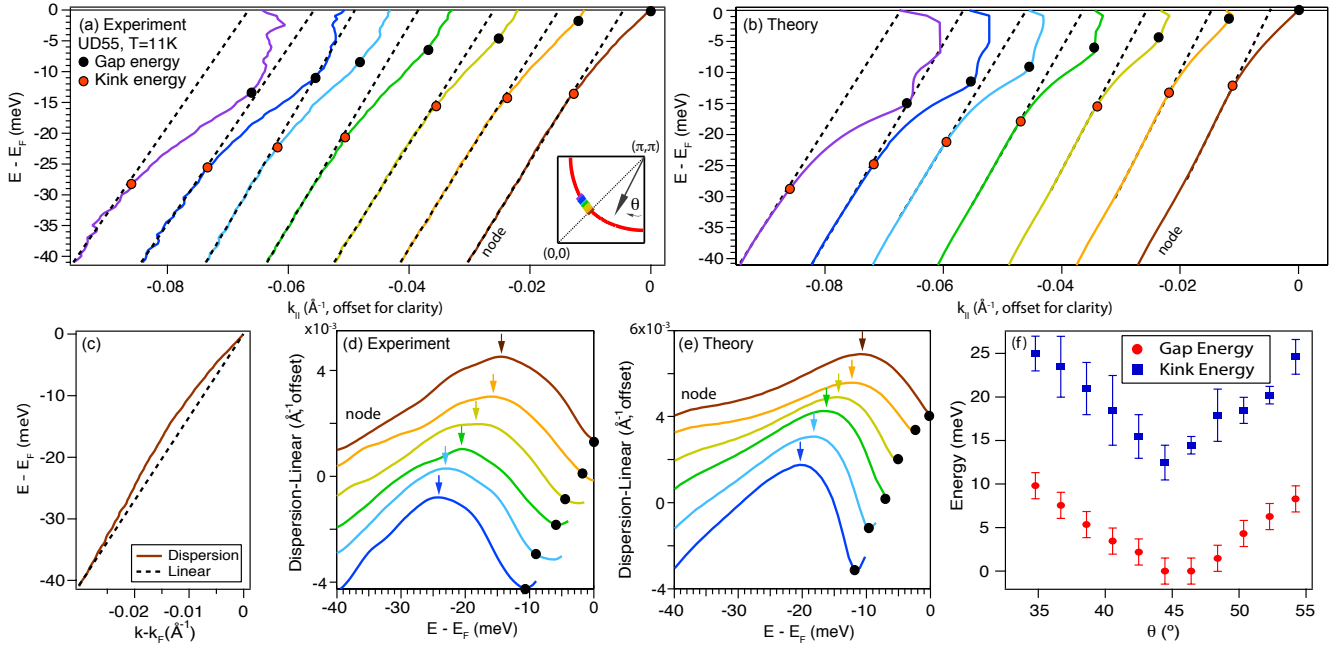


FIG. 4: (Color online) Low energy kink away from node (UD55, 11K). (a) MDC dispersions at node (rightmost) and away from the node, offset horizontally for clarity. Black circle represents gap energy, which is determined by fitting symmetrized data to a minimal model.²⁷ Red circle defines the approximate low-energy kink position, as determined by where the measured dispersion deviates from v_{mid} . (b) MDC dispersions obtained from the calculated $A(\mathbf{k}, \omega)$. (c) A sketch of how the kink position can be further quantified by subtracting a linear offset from the dispersion (shown here for nodal cut) between the gap energy and 40 meV. (d) Difference in \mathbf{k} between dispersion and dotted line in (c) for cuts from the node (top) and moving away from the node (towards the bottom). The data has been smoothed over 20 iterations and the curves have been offset vertically for clarity. Black dots indicate the gap energies and arrows mark peaks of these curves, determined from derivative after smoothing. (e) The difference in \mathbf{k} between the MDC dispersion and linear dispersion as in (d) but obtained from the calculated $A(\mathbf{k}, \omega)$. (f) Momentum dependence of gap and kink energies, the latter determined by method in (c).

As can be seen in the experimental data, as cuts are taken progressively further from the node both the superconducting gap and kink position shift to higher energies. This behavior is also reflected in the linear bare band subtraction, shown in Figs. 4d and is qualitatively reproduced by the model calculations. The momentum dependence of both energy scales are summarized in Fig. 4f, which shows a clear, constant offset between the local value of the gap and the kink position, similar to a previous study.⁷ Fig. 4b shows the calculated MDC dispersions and Fig. 4e show the subtracted linear bare band (Fig. 4c) obtained from applying the same procedures to the calculated spectral functions. The agreement between the theory and experiment is excellent and show that a strong coupling to the in-plane acoustic branch also captures the momentum-dependence of the low-energy kink.

Our results indicate that the acoustic modes couple to the lattice in a strongly doping and momentum-dependent way, which have a number of interesting implications and general consequences for these and other phonon modes. As the Coulomb interaction may dramatically alter the momentum-dependence of lattice effects, which become more pronounced as the screening length increases, the effect on transport can be substantial.²³ Due to the large forward scattering peak, coupling to the

acoustic branch may become less prominent in transport measurements apart from its overall renormalization of the Fermi velocity, as noted in a previous study (Ref. 9). Importantly, the $d_{x^2-y^2}$ pairing interaction from phonons can be dramatically changed whereby the screened e-ph interaction which favors large momentum scattering can become more peaked at small \mathbf{q} as screening breaks down and therefore might not be detrimental to d -wave pairing. This implies that the acoustic modes may in fact help d -wave pairing, in conjunction with electrons' coupling to c -axis and bond-stretching modes, in a way that would not be captured in fully itinerant and weak coupling scenarios. This further highlights the need to consider lattice effects and coupling to the full spectrum of oxygen phonon modes in order to obtain a complete understanding of the physics of the high- T_c cuprates.

The authors thank B. Moritz, R. He, E. van Heumen, N. C. Plumb and D. Dessau for useful discussions. This work was supported by the US Department of Energy, Office of Basic Energy Sciences under contract No. DE-AC02-76SF00515 and DE-FG03-01ER45929-A001. S. J. would like to acknowledge financial support from NSERC and the Foundation for Fundamental Research on Matter. Computational resources were provided by the Shared Hierarchical Academic Computing Network.

-
- ¹ F. Ronning *et al.*, Phys. Rev. B **71**, 094518 (2005);
- ² K. M. Shen *et al.*, Phys. Rev. B **75**, 075115 (2007).
- ³ R. Heid *et al.*, Phys. Rev. Lett. **100**, 137001 (2008).
- ⁴ F. Giustino, M. L. Cohen and S. G. Louie, Nature **452**, 975 (2008).
- ⁵ D. Reznik *et al.*, Nature **455**, E6 (2008).
- ⁶ W. Zhang *et al.*, Phys. Rev. Lett. **100**, 107002 (2008).
- ⁷ J. D. Rameau *et al.*, Phys. Rev. B **80**, 184513 (2009).
- ⁸ N. C. Plumb *et al.*, Phys. Rev. Lett. **105**, 046402 (2010).
- ⁹ I. M. Vishik *et al.*, Phys. Rev. Lett. **104**, 207002 (2010).
- ¹⁰ H. Anzai *et al.*, Phys. Rev. Lett. **105**, 227002 (2010).
- ¹¹ A. Lanzara *et al.*, Nature **412**, 6846 (2001).
- ¹² S. Johnston *et al.*, Adv. Cond. Mat. Phys. **2010**, 968304 (2010) and references therein.
- ¹³ T. P. Devereaux *et al.*, Phys. Rev. Lett. **93**, 117004 (2004).
- ¹⁴ W. S. Lee *et al.*, Phys. Rev. B **75**, 195116 (2007).
- ¹⁵ M. R. Norman *et al.*, Phys. Rev. Lett. **79**, 3506 (1997).
- ¹⁶ P. D. Johnson *et al.*, Phys. Rev. Lett. **87**, 177007 (2001).
- ¹⁷ S. V. Borisenko *et al.*, Phys. Rev. Lett. **96**, 117004 (2006).
- ¹⁸ T. Dahm *et al.*, Nature Physics **5**, 217 (2009).
- ¹⁹ N. N. Kovaleva, *et al.*, Phys. Rev. B **69**, 054511 (2004).
- ²⁰ A. W. Sandvik, D. J. Scalapino, and N. E. Bickers, Phys. Rev. B **69**, 094523 (2004).
- ²¹ E. G. Maksimov, O. V. Dolgov, and M. L. Kulić, Phys. Rev. B **72**, 212505 (2005).
- ²² G. D. Mahan, *Many-Particle Physics*, 2nd Ed. Plenum Press, New York (1990).
- ²³ S. Johnston *et al.*, Phys. Rev. B **82**, 064513 (2010).
- ²⁴ M. Eschrig and M. R. Norman, Phys. Rev. Lett. **85**, 3261 (2000). We apply a rigid shift to obtain $\langle n \rangle = 0.9$ and an overall renormalization of $Z = 0.9$.
- ²⁵ S. L. Chaplot, *et al.*, Phys. Rev. B **52**, 7230 (1995).
- ²⁶ M. L. Kulić and R. Zeyher, Phys. Rev. B **49**, 4395 (1994); R. Zeyher and M. L. Kulić, Phys. Rev. B **53**, 2850 (1996); Z. B. Huang *et al.*, Phys. Rev. B **68**, 220507(R) (2003);
- ²⁷ M. R. Norman, M. Randeria, H. Ding and J. C. Campuzano, Phys. Rev. B **57**, R11093 (1998).